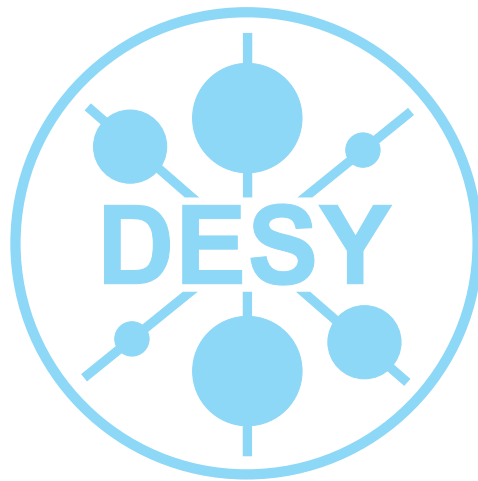


# DESY Summer Students Project

## Structure and Dynamics of highly-charged Colloidal Systems



Johannes Knebel (University of Rostock)

Ina Schneider (University of Regensburg)

Supervisor: Christian Gutt

16.09.2008

# Contents

<b>1</b>	<b>Introduction</b>	<b>3</b>
<b>2</b>	<b>Colloidal Systems</b>	<b>4</b>
2.1	Methyl Methacrylate Particles: F1SiMa . . . . .	5
2.2	Silica Particles: SiO <sub>2</sub> . . . . .	6
<b>3</b>	<b>Dynamic Light Scattering</b>	<b>7</b>
3.1	Scattering Theory . . . . .	8
3.1.1	First BORN Approximation . . . . .	8
3.1.2	Statistical Access to the Intensity: Static Structure Factor	9
3.1.3	Form Factor . . . . .	11
3.2	Static Measurements . . . . .	13
3.3	Dynamic Measurements . . . . .	14
<b>4</b>	<b>Experimental Setup</b>	<b>18</b>
<b>5</b>	<b>Measurements and Results</b>	<b>19</b>
5.1	Determination of the Radius . . . . .	19
5.2	Analysis of the Structure Factor and the Hydrodynamics . . . . .	23
5.2.1	Structure Factor . . . . .	23
5.2.2	Hydrodynamics . . . . .	27
<b>6</b>	<b>Conclusion</b>	<b>33</b>

**Abstract**

We used Dynamic Light Scattering to investigate colloidal FSiMa- and SiO<sub>2</sub>-systems. The dependence of the particles' radius on the concentration of KCl was investigated. Furthermore the static structure factor  $S(q)$  of FSiMa-colloids for several KCl concentrations was determined as well as the collective diffusion coefficient  $D_0/D(q)$ . From this, the hydrodynamic function was extracted.

## 1 Introduction

Everybody knows colloidal suspensions from the daily life. Paints and inks for example consist of pigments soluted in water or oil and also soaps, greases and blood are colloidal systems.

From the point of view of a chemist, the structure of colloids is enormously complicated but in physics, one can assume the particles to be spherical and without an inner structure. The investigation of such systems can help us to understand the processes of phase transitions like melting, freezing and also the glass transition, which are only rarely known so far.

Dynamic light scattering is besides X-ray photon correlation spectroscopy a very important and efficient means to investigate colloidal solutions. It gives us the possibility to gain insight into the structure and the dynamics of the systems.

## 2 Colloidal Systems

A colloidal solution consists out of particles in the  $\mu m \dots nm$  – range dispersed in a molecular liquid. To avoid agglomeration of the particles, a stabilization of the particles is necessary. This stabilization is usually realised in two ways. One possibility is the steric stabilization by polymer chains at the surface of the particles (see fig. 2.1). The overlap of the polymer layers causes an entropic repulsive force. This stabilization process can be modelled by a hard-sphere-potential between the particles in the solvent.

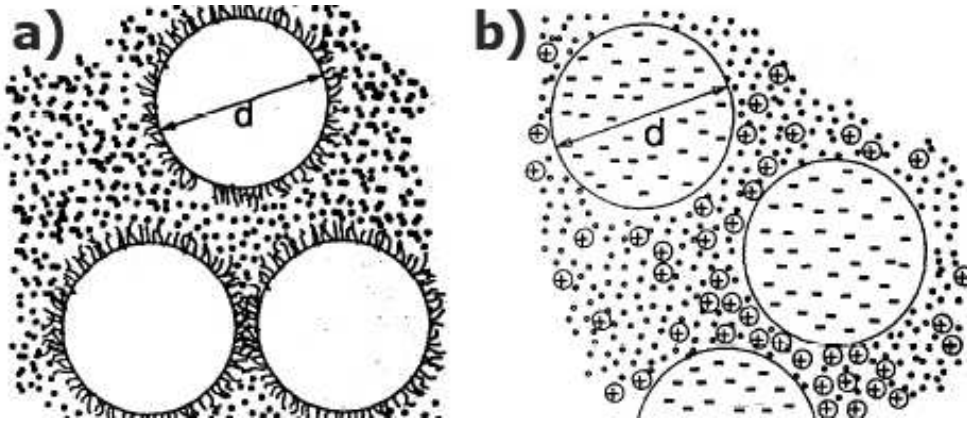


Figure 2.1: Stabilization processes: a) Entropic repulsion modelled by a hard-sphere-potential and b) COULOMB repulsion characterized by a Yukawa potential.

The other stabilization process is realized by surface charges (see fig. 2.1) and can be described with the screened COULOMB potential, also known as YUKAWA or DEBYE potential:

$$V(r) \propto \frac{e^{-\kappa r}}{r} , \quad (2.1)$$

with the inverse screening length  $\kappa$ .

Furthermore, the stabilization can be influenced by the temperature and the concentration of the colloids in the suspension.

In our experiments we used a FSiMa system, a methyl methacrylate polymer, and a suspended silica particle system. Both colloidal suspensions are charge stabilized.

## 2.1 Methyl Methacrylate Particles: F1SiMa

F1SiMa is produced by polymerization of the monomer methyl methacrylate. During this process different parameters can be tuned to determine the length of the polymer chains. By using crosslinking molecules these chains create a spherical network.

The Si-atoms are installed in the polymer in order to increase the signal in the scattering experiment, F1-atoms are introduced to enlarge the electronegativity of the particles due to charge stabilization.

The whole molecule acts like a big ion, interacting with its neighbor atoms through surface charges as mentioned above.

## 2.2 Silica Particles: SiO<sub>2</sub>

The silica particles are produced by the STÖBER synthesis. Tetraethoxysilane (TEOS) serves as a starting substance.

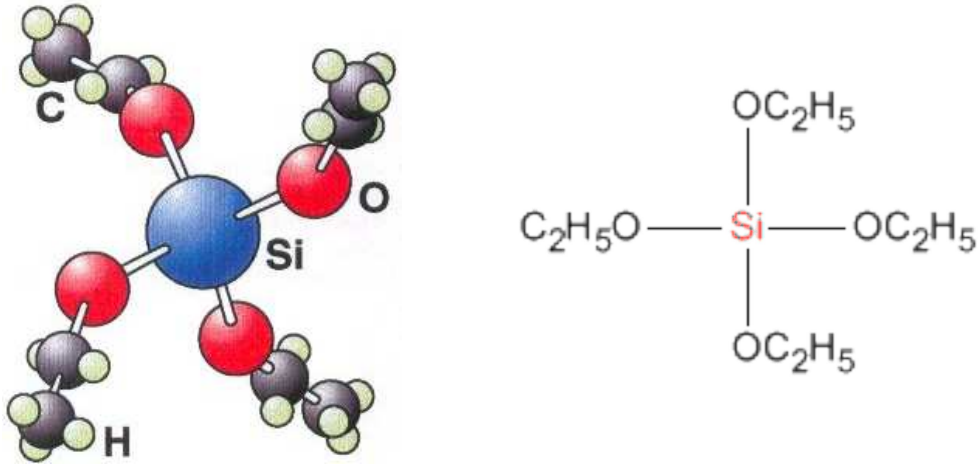
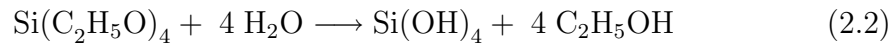
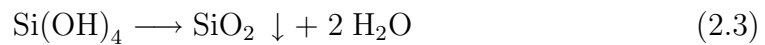


Figure 2.2: Constitution and structural formulae of Tetraethoxysilane (TEOS).

This monomer is converted into siliconhydroxide by a hydrolysis reaction:



This process is followed by a condensation whereby the silica particles are precipitated:



The silica particles in water also form charge stabilized spherical particles as said before.

### 3 Dynamic Light Scattering

Dynamic light scattering (DLS) is one of the most powerful experimental tools to investigate the dynamics of colloidal suspensions. The basic principle of such a scattering experiment is an incident coherent beam that impinges on a colloidal fluid and is scattered by its mesoscopic structures. The scattered intensity in the far field is fluctuating in time due to an fluctuating interference pattern at the place of the detector. The intensity also depends on the scattering angle  $\theta$  between the incident beam and the scattered beam (cf. figure 3.3).

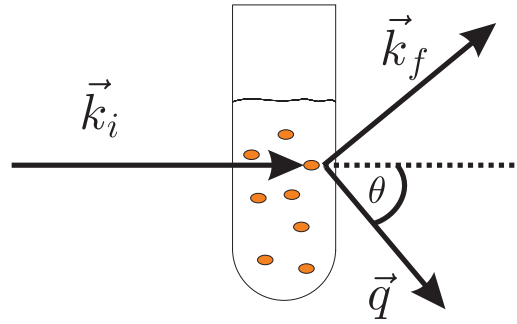


Figure 3.3: Sketch of a standard scattering experiment. The incident laser beam is scattered by the particles of the colloidal suspension. The scattered light is measured by a detector.

Since we are dealing with visible light, the photon energy is much smaller than the binding energy of the electrons. For weakly bound electrons, for example valence electrons, the accelerated electrons can be regarded as HERTZ dipoles emitting a secondary wave with the same wavelength as the stimulating primary wave. In this regime we can presume elastic light scattering, meaning  $|\vec{k}_i| = |\vec{k}_f| = k$  and therefore we have for the scattering vector  $\vec{q} = \vec{k}_i - \vec{k}_f$ :

$$q = \frac{4\pi n}{\lambda} \cdot \sin(\theta/2) \quad , \quad (3.4)$$

with  $n$  as the index of refraction and  $\lambda$  as the wavelength of the incident beam. DLS measures the fluctuating intensity as a time dependent intensity correlation function at a given spatial position that is related via eq. 3.4 to the scattering vector  $\vec{q}$  and to the momentum transfer  $\vec{p}_q = \hbar\vec{q}$ . From this, the structure and the dynamics of the colloidal system can be determined. For example, from the temporal decay of the intensity correlation function, the collective diffusion coefficient of the colloids can be obtained. However, this only holds as long as the light is not multiply scattered within the sample. That has to be taken into account for the experimental setup.

### 3.1 Scattering Theory

#### 3.1.1 First Born Approximation

In the standard scattering experiment (figure 3.3) the incoming beam is regarded as a planar wave  $\varphi_0(r)$ . In the scattering center the scattered wave  $\varphi_s(r)$  is produced and can be regarded as a spherical wave in the far-field-approximation. That means:

$$\varphi_s(r) \xrightarrow{r \rightarrow \infty} f(\vartheta, \phi) \frac{e^{i\vec{k}_f \cdot \vec{r}}}{r} ,$$

where  $f(\vartheta, \phi)$  is the scattering amplitude. With these boundary conditions the time-independent Schrödinger equation

$$\left( \frac{\vec{p}^2}{2m} + V(r) \right) \varphi(r) = E \varphi(r) \quad (3.5)$$

for

$$\varphi(r) = \varphi_0(r) + \varphi_s(r) \quad (3.6)$$

with  $V(r)$  as the scattering potential has to be solved. From this point, it is possible to rewrite  $\varphi(r)$  as an integral equation that is equivalent to eq. 3.5 including the boundary conditions:

$$\varphi(r) = e^{ikz} - \frac{m}{2\pi\hbar^2} \cdot \int d^3r' V(r') \frac{e^{ik|\vec{r}-\vec{r}'|}}{|\vec{r}-\vec{r}'|} \varphi(r')$$

In the far-field-approximation ( $r \rightarrow \infty$ ) this leads to

$$\varphi(r) \rightarrow e^{ikz} - \frac{e^{ikr}}{r} \frac{m}{2\pi\hbar^2} \cdot \int d^3r' V(r') e^{-ik(\vec{e}_r \cdot \vec{r}')} \varphi(r').$$

Comparing this result with eq. 3.6 one obtains for the scattering amplitude

$$f(\vartheta, \phi) = -\frac{m}{2\pi\hbar^2} \cdot \int d^3r' V(r') e^{-ik(\vec{e}_r \cdot \vec{r}')} \varphi(r').$$

Applying BORN's first approximation that holds for single scattering one finally gets the result

$$f^{(1)}(\vartheta, \phi) = -\frac{m}{2\pi\hbar^2} \cdot \int d^3r' V(r') e^{-i\vec{q} \cdot \vec{r}'}. \quad (3.7)$$

### 3.1.2 Statistical Access to the Intensity: Static Structure Factor

Assuming that the potential  $V(r)$  can be written as the sum of the potentials  $\sum_i V_{\text{atom}}(\vec{r} - \vec{R}_i)$  for atomic scattering centers placed at  $\vec{R}_i$ , it is now possible to calculate the intensity  $I(q)$  within the first BORN approximation (eq. 3.7):

$$I(q) \propto |f^{(1)}(\vartheta, \phi)|^2 = \left( \frac{m}{2\pi\hbar^2} \right)^2 \cdot |V(\vec{q})|^2 \cdot \sum_{i,j} e^{-i\vec{q}(\vec{R}_i - \vec{R}_j)} \quad (3.8)$$

where the FOURIER transform of the potential  $V(\vec{r})$  was introduced:

$$V(\vec{q}) = \int d^3r e^{i\vec{q}\cdot\vec{r}} \cdot V(\vec{r}) \quad (3.9)$$

Further, it makes sense to look at eq. 3.8 from the statistical point of view. It is possible to introduce the static structure factor that is defined as the spacelike FOURIER transform of the radial distribution function  $g(r)$ :

$$S(q) = \int d^3r e^{i\vec{q}\cdot\vec{r}} \cdot g(r) \quad , \quad (3.10)$$

whereas  $g(r)$  is defined as

$$g(r) = \frac{1}{n} \left\langle \frac{1}{N} \sum_{i,j}^N \delta(\vec{r} - [\vec{R}_i - \vec{R}_j]) \right\rangle \quad , \quad (3.11)$$

with the particle number  $N$  and the particle density  $n$ . The brackets  $\langle \cdot \rangle$  indicate an ensemble average. The static structure factor describes in general the ensemble correlations of the examined system. Figure 3.4 shows a typical behaviour of the structure factor  $S(q)$  for a concentrated colloidal system. The exact functional form of the structure factor depends on the nature of the interaction, described by the potential, the temperature of the colloidal suspension and the concentration of the colloids. For example, a strong interaction would cause the particles to form some kind of regularly structure and the static structure factor would display a maximum at  $q_{\text{max}}$ . This value is related to the mean interparticle distance  $d$  via

$$d = \frac{2\pi}{q_{\text{max}}} \quad (3.12)$$

Furthermore, the full width at half maximum (FWHM) of the first peak of the structure factor is connected to the correlation length in the examined system. The larger the FWHM the smaller the correlation length.

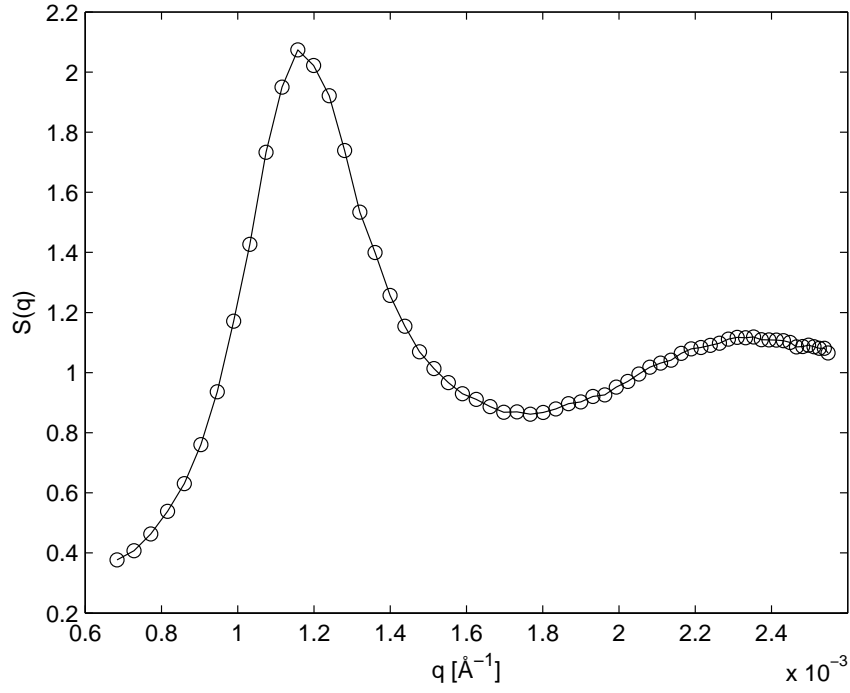


Figure 3.4: Typical static structure factor of a concentrated colloidal suspension.

Inserting eq. 3.13 into eq. 3.10 one obtains

$$S(q) = \frac{1}{nN} \left\langle \sum_{i,j}^N e^{-i\vec{q}(\vec{R}_i - \vec{R}_j)} \right\rangle. \quad (3.13)$$

Applying ensemble averaging of the intensity  $\langle I(q) \rangle$  eq. 3.8 leads to

$$\langle I(q) \rangle \propto |V(\vec{q})|^2 \cdot S(q). \quad (3.14)$$

### 3.1.3 Form Factor

It is often more common to characterize an atomic system by the electron density  $\rho(r)$  instead of the scattering potential  $V(r)$ . These two quantities are connected by the POISSON-equation

$$\Delta_{\vec{r}}V(r) = -\frac{\rho(r)}{\epsilon_0}. \quad (3.15)$$

Applying GREEN's second identity

$$\int_U dV (\psi \Delta_{\vec{r}} \Psi - \Psi \Delta_{\vec{r}} \psi) = \oint_{\partial U} dS \left( \psi \frac{\partial \Psi}{\partial n} - \Psi \frac{\partial \psi}{\partial n} \right) \quad (3.16)$$

with  $\psi = V(r)$  and  $\Psi = -\frac{e^{i\vec{q}\cdot\vec{r}}}{|\vec{q}|^2}$ , the surface term on the right hand side of eq. 3.16 vanishes for adequate scatter potentials  $V(r)$  (for example the COULOMB potential) and the FOURIER transform of the potential  $V(q)$  can be identified with the FOURIER transform of the electron density  $\rho(q)$  called the form factor  $F(q)$ :

$$F(q) = \int d^3r e^{i\vec{q}\cdot\vec{r}} \cdot \rho(r) \quad (3.17)$$

leading to

$$V(q) \propto \frac{F(q)}{q^2}. \quad (3.18)$$

For example, the form factor for a pointlike particle results in  $F(q) = 1$  whereas a homogenous sphere with radius  $R$  leads to

$$F(q) \propto \frac{\sin(qR) - qR \cdot \cos(qR)}{(qR)^3}. \quad (3.19)$$

The form factor for a homogenous sphere is shown in figure 3.5.

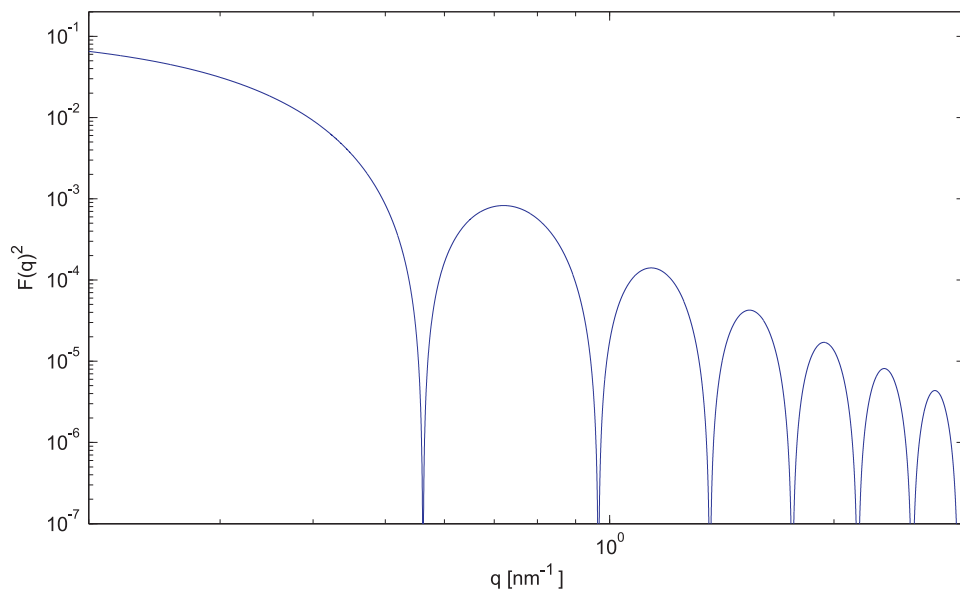


Figure 3.5: Form factor of a homogenous sphere.

## 3.2 Static Measurements

Going back to eq. 3.14 and applying the result from eq. 3.18 one finally has

$$\langle I(q) \rangle \propto \frac{F(q)^2 \cdot S(q)}{q^4}. \quad (3.20)$$

From this, one can extract the static structure factor experimentally by assuming the ergodic hypothesis saying that the average over time of the intensity  $\langle I \rangle_t$  equals the average over the statistical ensemble  $\langle I \rangle$ . Since only the time average over the intensity is accessible in experiments, one has to postulate this theorem. By doing so, one can extract information about the structure of the colloidal suspension and the particles from static measurements.

### 3.3 Dynamic Measurements

To gain insight into the dynamics of the colloids it is necessary to look from another point of view on the intensity measurement. As mentioned before, the detector measures the fluctuating intensity caused by the spatially inhomogeneous refractive index or electron density in the colloidal suspension that results in an intensity distribution of dark and bright regions in the far field, also known as speckle pattern. This pattern changes in time due to the dynamics in the sample and therefore the measured intensity at this point fluctuates in time.

By applying photon correlation spectroscopy (PCS) the intensity autocorrelation function (IAF) is introduced:

$$\langle I(q, t + \tau)I(q, t) \rangle_t = \lim_{T \rightarrow \infty} \frac{1}{T} \int_0^T dt I(q, t)I(q, t + \tau) \quad (3.21)$$

With  $I(q, t)$  as the time-dependent scattered intensity, it is possible to determine the dynamics of the colloidal system. The IAF and its relation to the temporal fluctuations in intensity is shown in figure 3.6. The correlation starts with a maximum value of  $\langle I^2 \rangle$  and decreases in time to  $\langle I \rangle^2$  with the characteristic decay time  $\tau_c$ .

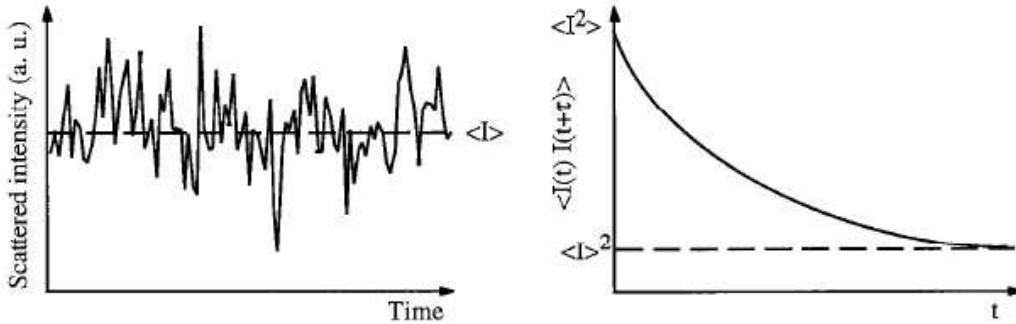


Figure 3.6: Fluctuations in the scattered intensity and the intensity autocorrelation function.

For example, if the time compared to the typical time scale of configurational changes of the colloids is small, the intensity will be correlated with the initial intensity. In contrast to that, no correlation will be measured at large times.

In theory, the fluctuating amplitude of the electric field can be expressed by the quantity  $g_1$ :

$$g_1(q, \tau) = \frac{\langle E^*(q, \tau)E(q, 0) \rangle}{\langle |E(q, \tau)|^2 \rangle} \quad (3.22)$$

In a DLS experiment the IAF of the intensity is measured as the so called  $g_2$ -function

$$g_2(q, \tau) = \frac{\langle I(q, \tau)I(q, 0) \rangle}{\langle I(q, \tau) \rangle^2} \quad (3.23)$$

where also the ergodic hypothesis is assumed. Further, the relation  $I(q, \tau) = E^*(q, \tau)E(q, \tau)$  connects  $g_1$  and  $g_2$ . For a Gaussian distribution of the field amplitude  $E(q, \tau)$  of zero mean this relation can be specified since Gaussian variables of zero mean are completely described by their second moment:

$$\begin{aligned} \langle I(q, \tau)I(q, 0) \rangle &= \langle E^*(q, 0)E(q, 0)E^*(q, \tau)E(q, \tau) \rangle \\ &= \langle E^*(q, 0)E(q, 0) \rangle \langle E^*(q, \tau)E(q, \tau) \rangle \\ &\quad + |\langle E(q, 0)E(q, \tau) \rangle|^2 \\ &\quad + |\langle E(q, 0)E^*(q, \tau) \rangle|^2 \\ &= \langle I(q, 0) \rangle \langle I(q, \tau) \rangle + |\langle E(q, 0)E^*(q, \tau) \rangle|^2 \end{aligned}$$

whereas the second term in the second step can be neglected due to time-averaging over the Gaussian field amplitude. Applying this result one can therefore write with eq. 3.22 and eq. 3.23

$$g_2(q, \tau) = 1 + \beta^2 \cdot |g_1(q, \tau)|^2 \quad (3.24)$$

which is known as the SIEGERT relation. The parameter  $\beta$  describes the contrast that is usually close to  $\beta = 1$  in standard DLS experiments. In case of cross-correlation this reduces to  $\beta = 0,25$ .

In case of monodisperse spherical particles,  $g_1$  can be written as follows:

$$g_1(q, \tau) = S(q, \tau) \frac{H(q)}{S(q)} \quad (3.25)$$

with  $S(q, \tau)$  as the dynamic structure factor,  $S(q)$  as the static structure factor known from section 3.1.2 and the hydrodynamic function  $H(q)$  that describes the hydrodynamic interactions in the suspension.

For colloidal systems with negligible interactions, for example highly diluted colloidal suspensions, a relationship between the  $g_1$ -function and the collective free diffusion coefficient  $D_0$  can be derived:

$$g_1(q, \tau) \propto e^{-D_0 q^2 \tau}. \quad (3.26)$$

Together with the SIEGERT relation (eq. 3.24) it follows that

$$g_2(q, \tau) - 1 \propto e^{-2D_0 q^2 \tau}, \quad (3.27)$$

meaning that the dynamics of the examined system (represented by  $D_0$ ) can be characterized by measuring  $g_2$ .

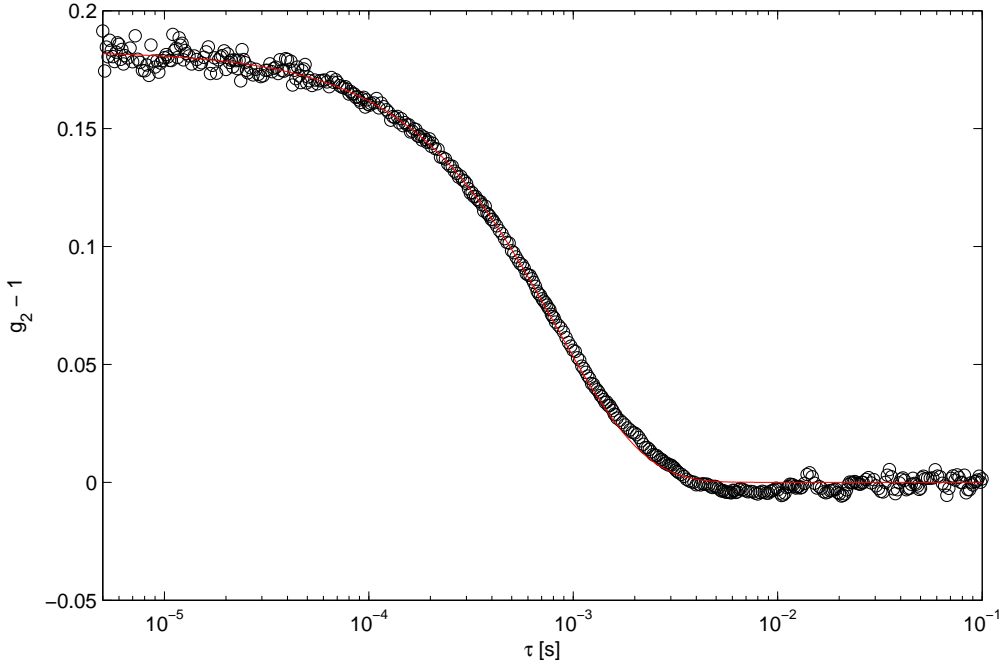


Figure 3.7: Example of a measured  $g_2 - 1$  function for a colloidal system plotted on logarithmic time scale. The exponential decay represents the data quite well.

Figure 3.7 shows a typical measurement of  $g_2(q, \tau) - 1$ .

Using the EINSTEIN-STOKES equation  $D = \mu k_B T$  with  $\mu = 1/f$  as the mobility of the particles and  $f = 6\pi\eta R_H$  as the friction coefficient, following equation for  $D_0$  can be obtained:

$$D_0 = \frac{k_B T}{6\pi\eta R_H} , \quad (3.28)$$

where  $R_H$  describes the hydrodynamic radius of the particles and  $\eta$  the viscosity of the suspending medium. For highly diluted samples the hydrodynamic radius  $R_H$  equals the geometrical particle radius  $R$ . By determining  $D_0$  it is then possible to calculate the radius of the solved particles.

In the presence of particle interaction one usually analyses  $g_1$  in terms of a cumulant expression:

$$g_1(q, \tau) = e^{-\Gamma_1(q)\tau + \Gamma_2(q)\tau^2 + \dots}$$

The initial decay of  $g_1$  can be regarded as the collective short time diffusion coefficient  $D(q)$  of the colloidal suspension whereas  $\Gamma_1(q) = D(q) \cdot q^2$ . Thus, one gets for the short time behaviour of  $g_1$ :

$$g_1(q, \tau) = e^{-D(q)q^2\tau} \quad (3.29)$$

and for the short time behaviour of  $g_2$ :

$$g_2(q, \tau) - 1 \propto e^{-2D(q)q^2\tau} \quad (3.30)$$

It can be shown that the short time diffusion coefficient  $D(q)$  is given by

$$D(q) = D_0 \cdot \frac{H(q)}{S(q)} \quad , \quad (3.31)$$

with the hydrodynamic function  $H(q)$  and the static structure factor  $S(q)$  as mentioned above.

## 4 Experimental Setup

As a light source for the dynamic light scattering experiment, a 633 nm HeNe-laser is used. To adjust the intensity of the incoming laser beam, there are two rotatable wheels with several absorption filters of different optical densities. After the beam has passed these filters, its intensity is measured by a photo diode and it gets split-up into two beams. This splitting-up process is necessary to make a later cross-correlation possible, to suppress the contribution of multiple scattered light to the measured data as mentioned before.

A lens system is used to focus the two laser beams onto the sample. The sample itself is filled into a quartz-capillary which is then placed into a decaline chamber whose temperature can be adjusted by the use of a chiller. Since we did not investigate any temperature dependency of the behaviour of the colloidal systems on the temperature, we always set the temperature to 20°C. The beams are diffracted from the sample and their intensities are measured by a detector which is attached to a goniometer. By the use of this goniometer, it is possible to measure the intensities in an angular range of  $\theta = 30^\circ$  to  $\theta = 150^\circ$ .

A hardware auto-correlator is calculating the auto-correlation function  $g_2(q, \tau) - 1$  of the signal measured by the detector.

The intensity  $I(q, t)$  measured by the detector and the auto-correlation function  $g_2(q, \tau) - 1$  calculated by the auto-correlator is now the starting point for all of our further data analysis.

The experimental setup is illustrated in figure 4.8.

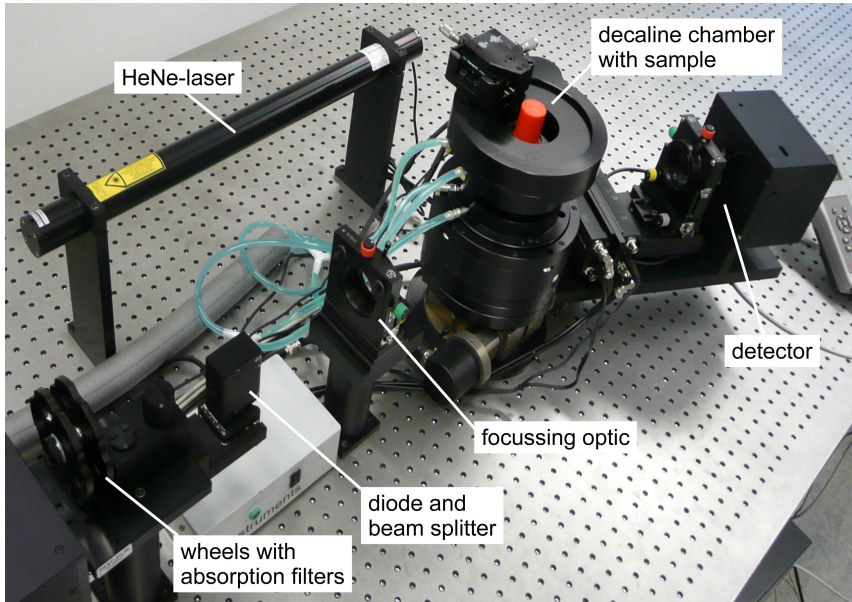


Figure 4.8: Picture of the experimental setup.

## 5 Measurements and Results

### 5.1 Determination of the Radius

The first part of our work consisted of the determination of the radius of the colloids in different samples. We used two different FLSiMa-systems, *FLSiMa020507* and *FLSiMa110708*, and *SiO<sub>2</sub>280708*, the SiO<sub>2</sub>-system that we prepared on our own. The aim of the measurements was to investigate if there is any connection between the dynamic radius of the colloids and the concentration of salt in the solvent.

First we investigated the *FLSiMa020507*-system. To make sure that there are no particle interactions so that the diffusion constant is independent of the scattering vector  $\vec{q}$ , the system was diluted 1:100 in water. Now we prepared samples with concentrations of KCl in the range between  $1\mu\text{M} - 2000\mu\text{M}$ .

From the auto-correlation function calculated by the hardware auto-correlator, we were able to identify the characteristic time  $\tau_c(q)$  for each sample as a function of  $q$ , that we could derive from the scattering angle  $\theta$  by the relation given via equation 3.4.

Now we plotted  $\Gamma(q^2) = D(q) \cdot q^2$  which is the inverse of the characteristic time  $\tau_c$ . The slope of this graph is equal to the diffusion constant  $D_0$ . Figure 5.9 shows the result that we obtained for a KCl-concentration of  $200\mu\text{M}$ .

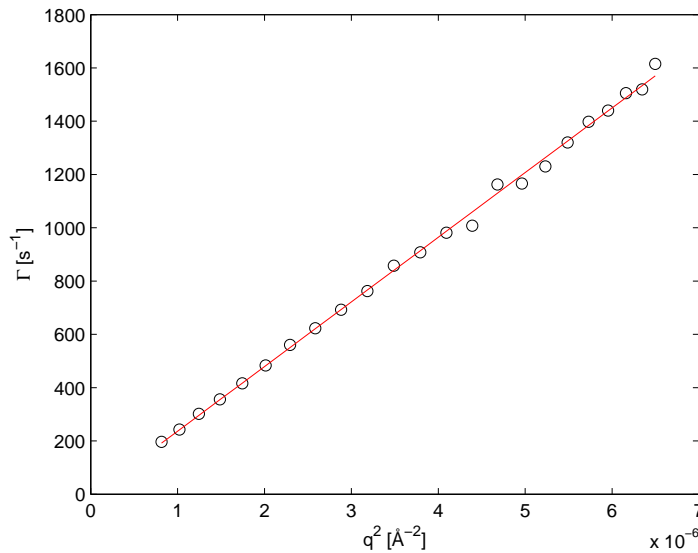


Figure 5.9:  $\Gamma(q^2)$  plotted for the *FLSiMa020507*-system diluted 1:100 in water with a KCl-concentration of  $200\mu\text{M}$ .

The slope and thereby also the diffusion constant for this sample is  $2.43 \cdot 10^{-12} \frac{\text{m}^2}{\text{s}}$ . The EINSTEIN diffusion equation 3.28 yields a radius of the particles of  $(88.38 \pm 0.88)\text{nm}$ , assuming the viscosity of water to be  $1.0 \cdot 10^{-3} \frac{\text{Ns}}{\text{m}^2}$  for a temperature of  $20^\circ\text{C}$ .

After determining the radius of the colloids in the different samples, we were able to plot the radius as a function of the concentration of KCl. The result is shown in figure 5.10.

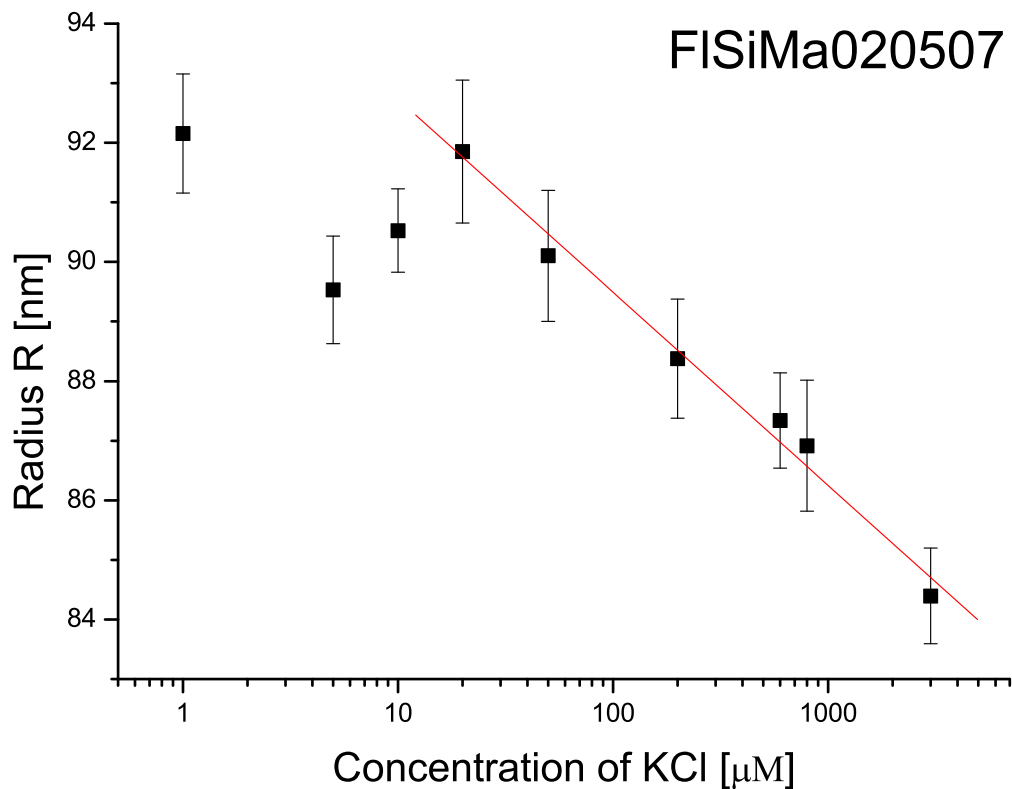


Figure 5.10: The radius of the colloids in the FLSiMa020507-system, plotted as a function of the KCl-concentration.

As one can see from the plot, the radius of the colloids is decreasing with the increasing concentration of KCl, starting at a concentration of about  $20\mu\text{M}$ .

We did the same kind of measurement and analysis for a second FLSiMa-system: *FLSiMa110708*. The result is shown in figure 5.11.

The plot illustrates, that this FLSiMa-system shows pretty much the same behaviour as the FLSiMa-system we investigated before. The radius is again de-

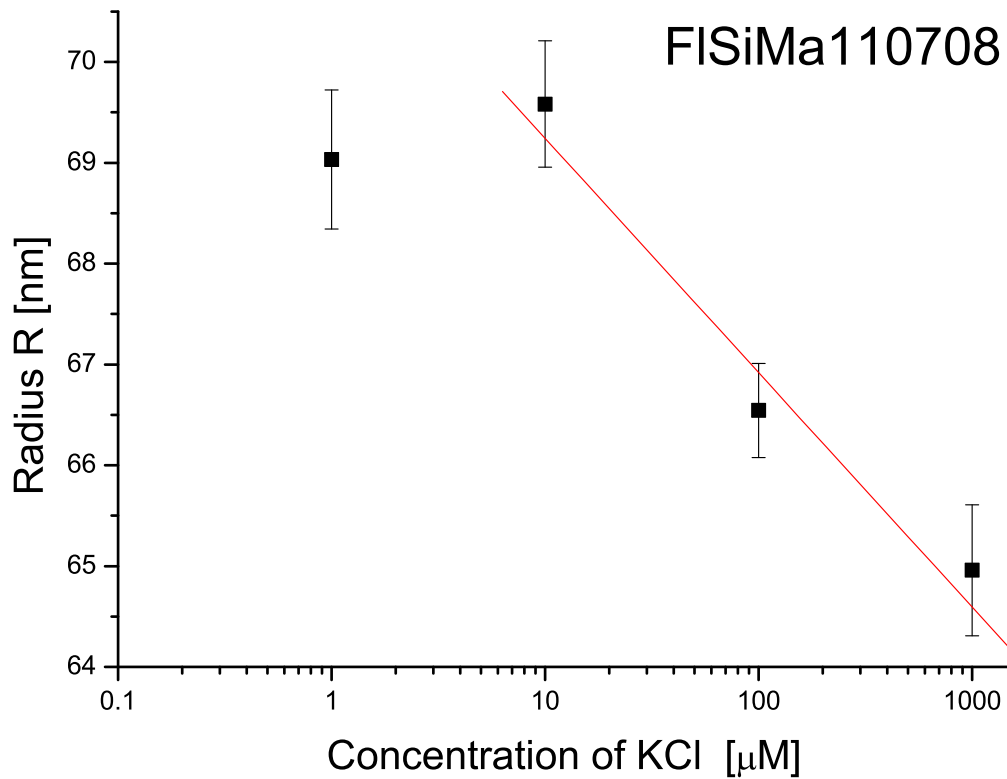


Figure 5.11: The radius of the colloids in the FLSiMa110708-system, plotted as a function of the KCl-concentration.

creasing with the increasing concentration of salt, starting at a concentration of about  $10\mu\text{M}$ .

Thinking about an explanation for this behaviour, one has to bear in mind that the viscosity of the solvent, which appears in the EINSTEIN diffusion equation as well, was assumed to be constant when calculating the radius of the particles. Probably this assumption is not realistic and the seeming change of the radius is just resulting from a change in the viscosity that occurs when salt is added to the system. Unfortunately, we did not have the possibility to measure the viscosity of our samples, what might have been a way to figure out whether the results of the calculation of the radius are only arising from a change in viscosity. Another alternative would have been to determine the radius by static means, investigating the form factor of the colloidal systems, which is not possible with the used experimental setup since the wavelength of the laser is too long.

After investigating the radius of the colloids in the FLSiMa-systems, we turned to the  $\text{SiO}_2$ -system. This time, we varied the concentration of KCl in a range of  $0.001\mu\text{M} - 3000\mu\text{M}$ . Figure 5.12 shows the results of the calculations for that system.

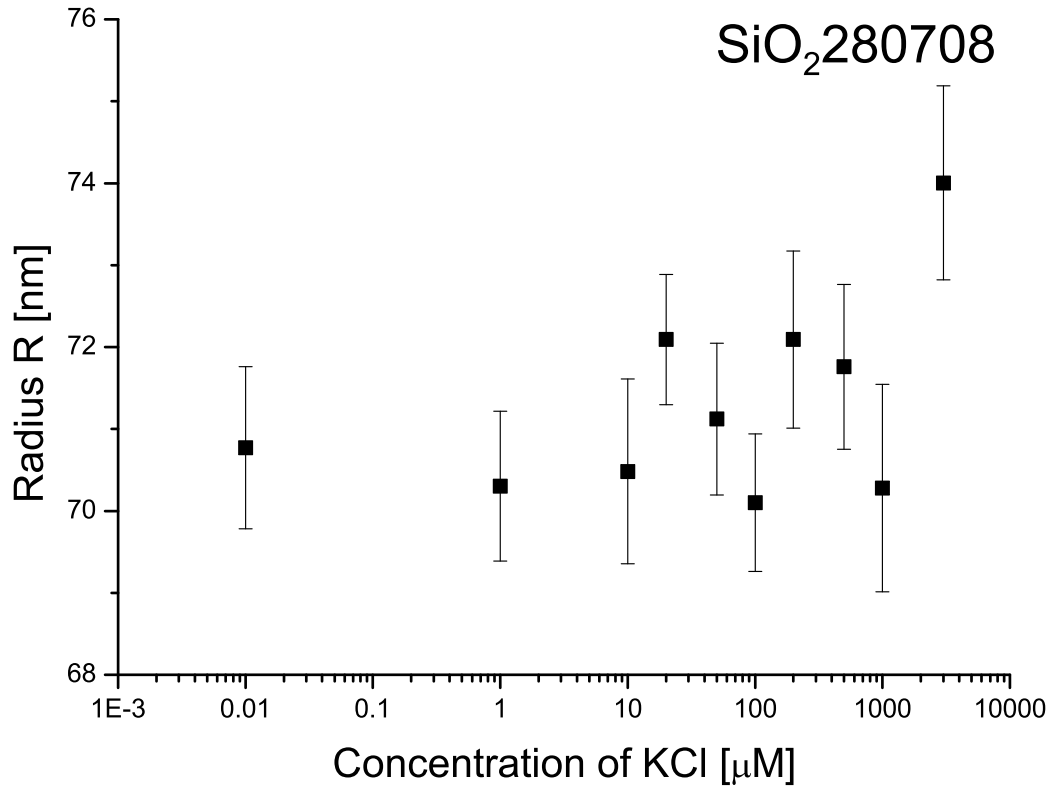


Figure 5.12: The radius of the colloids in the  $\text{SiO}_2$ -system, plotted as a function of the KCl-concentration.

As one can see from the plot, we weren't able to figure out any kind of dependency of the particle radius on the concentration of salt.

## 5.2 Analysis of the Structure Factor and the Hydrodynamics

### 5.2.1 Structure Factor

As shown before, for the mean intensity measured in the DLS-experiment and the structure- and form-factor, there is the relation given in equation 3.20. If we now want to determine the structure factor of our sample, we can make use of this relation in the following way: Additional to the sample whose structure factor we want to determine, we prepare a second sample from the same sample system but with a very high concentration of salt. In such a sample, we can assume the structure factor to be one as the COULOMB potential between the colloids gets screened by the ions, so that there are no more particle interactions. Furthermore, we can assume that the form factor of the sample we are investigating and the form factor of the sample with the high concentration of salt are identical.

If we now divide the mean intensity  $\langle I(q) \rangle_t$  that we measured for our sample by the mean intensity  $\langle I_0(q) \rangle_t$  measured for the sample with the high concentration of salt, we get the following simple relation:

$$S(q) = \frac{\langle I(q) \rangle_t}{\langle I_0(q) \rangle_t}. \quad (5.32)$$

In this way, we determine the structure factor of our samples.

In our work, we investigated the structure factor of the *FLSiMa070507*-system. This time, we used a concentrated solution. We prepared samples with concentrations of KCl between  $5\mu\text{M} - 200\mu\text{M}$ . In each case, we measured the mean intensity and divided it by the mean intensity that we measured for the  $200\mu\text{M}$ -sample. Figure 5.13 shows the data that we got for the mean intensities of the  $5\mu\text{M}$ - and the  $200\mu\text{M}$ -sample.

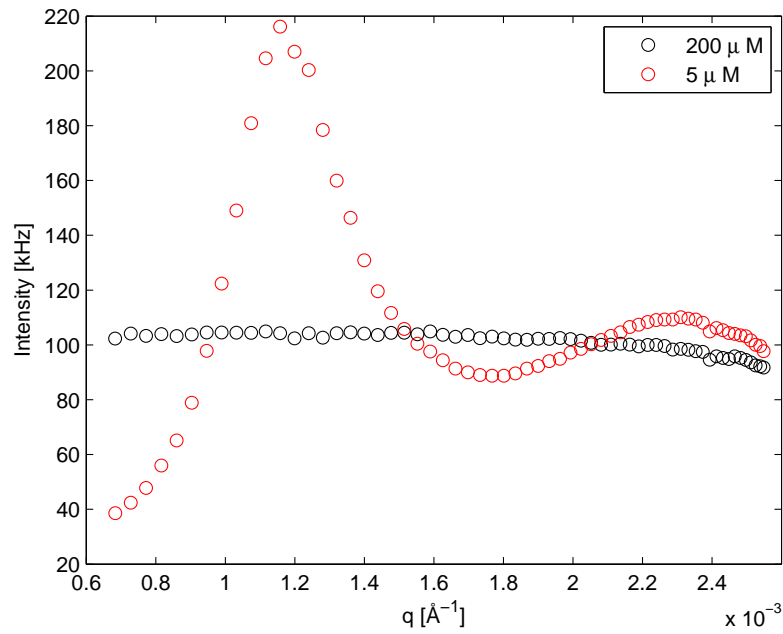


Figure 5.13: The mean intensities measured for the  $5\mu\text{M}$ - and the  $200\mu\text{M}$ -sample as a function of  $q$ .

As one can see, there is a very pronounced peak in the mean intensity measured for the  $5\mu\text{M}$ -sample. For the  $200\mu\text{M}$ -sample, there is no more peak in the mean intensity observable. The mean intensity is constant as a function of  $q$ . This assures us in our assumption, that there are no more particle interactions in this sample but only Brownian motion.

In the next step we divided the mean intensity measured for each of our samples by the mean intensity of the  $200\mu\text{M}$ -sample. Figure 5.14 shows the result of these calculations.

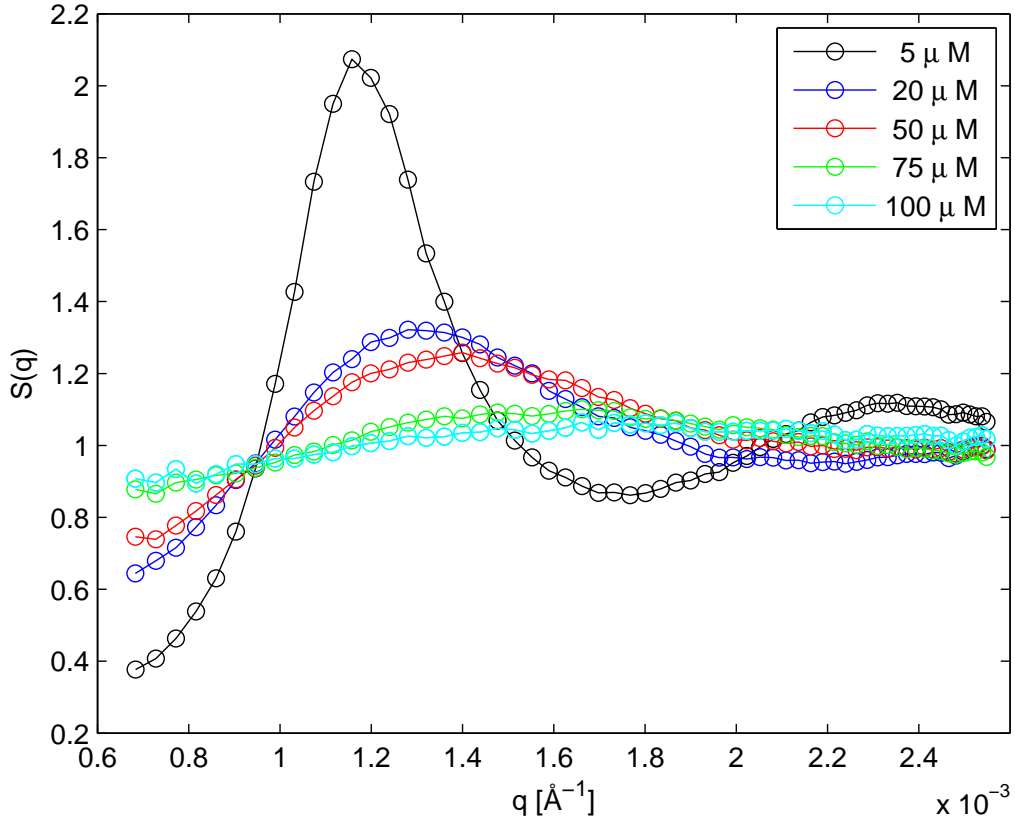


Figure 5.14: The calculated structure factors for the  $5\mu\text{M}$ - $200\mu\text{M}$ -samples of the *FlSiMa070507*-system plotted as a function of  $q$ .

In the theory of colloidal systems, the value of  $S(q_{\text{max}})$  serves as an indicator for the phase. The phase transition between the liquid and the glassy state takes place at about  $S(q_{\text{max}}) \approx 2.6$ . Thus we can see from the plot, that even in the case of the  $5\mu\text{M}$ -sample, we are still dealing with a liquid system.

We can also see from the plot, that  $q_{\text{max}}$  rises with the increase of the concentration of KCl. This means that the mean interparticle distance decreases. By adding salt, the COULOMB potential between the particles gets screened, whereby the repulsive force between them decreases. As a result, the equilibrium distance between the colloids gets smaller and  $q_{\text{max}}$  increases accordingly.

The next result we can see from the plot is that the FWHM of  $S(q)$  increases when adding salt to the system. As already mentioned, the COULOMB potential between the particles gets screened by the ions which means that the VAN-DER-WAALS interaction comes to the fore. As the COULOMB interaction is proportional to  $\frac{1}{r}$  while the VAN-DER-WAALS interaction is proportional to  $\frac{1}{r^6}$ , the

long-distance effect of the interactions disappears. As a consequence, the correlation length of the system decreases what explains the enhancement of the FWHM.

### 5.2.2 Hydrodynamics

The last part of our work was the investigation of the hydrodynamic function  $H(q)$ . The hydrodynamic function is defined as

$$H(q) = \frac{S(q)}{D_0/D(q)} \quad (5.33)$$

and gives us information about the interactions between the particles that are transmitted over the solvent, which is in our case water. The more  $H(q)$  approaches one, the less interactions are transmitted over the solvent.

We used the same FLSiMa-system as for the calculations of the structure factor and took the measuring data from the same samples as before with KCl concentrations of  $5\mu\text{M} - 200\mu\text{M}$ .

We obtained the structure factor of the samples as shown in chapter 5.2.1 and the diffusion function  $D(q)$  as shown in chapter 5.1 with the difference that it is now depending on  $q$  and is not a constant anymore.

Figure 5.15 shows the  $\Gamma(q^2)$  function that we obtained for the  $5\mu\text{M}$ -sample. The slope of this graph is equal to  $D(q)$ .

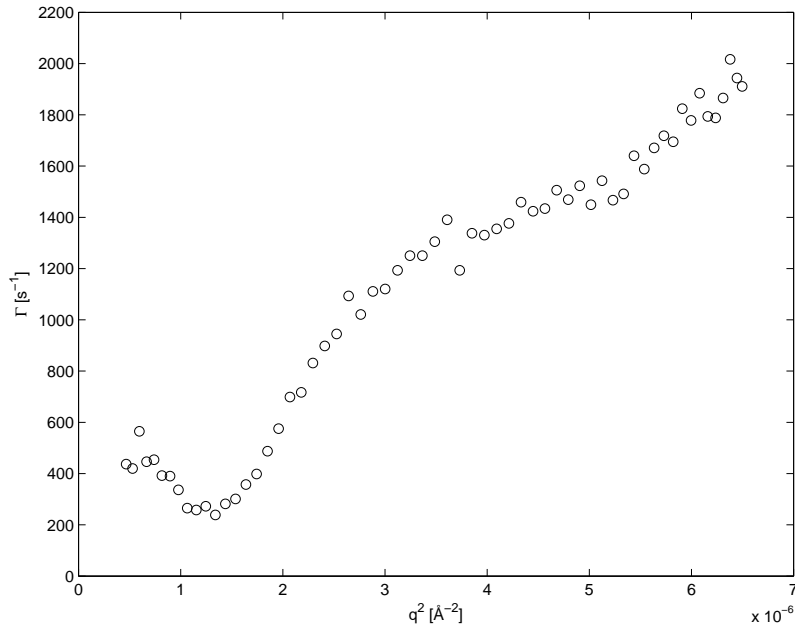


Figure 5.15:  $\Gamma(q^2)$  for the  $5\mu\text{M}$  FLSiMa070507 sample. From the slope of the function we can obtain the diffusion function  $D(q)$ .

$D_0$  is the diffusion constant that we calculated for the  $200\mu\text{M}$ -sample. The  $\Gamma(q^2)$  function for this sample is shown in figure 5.16.

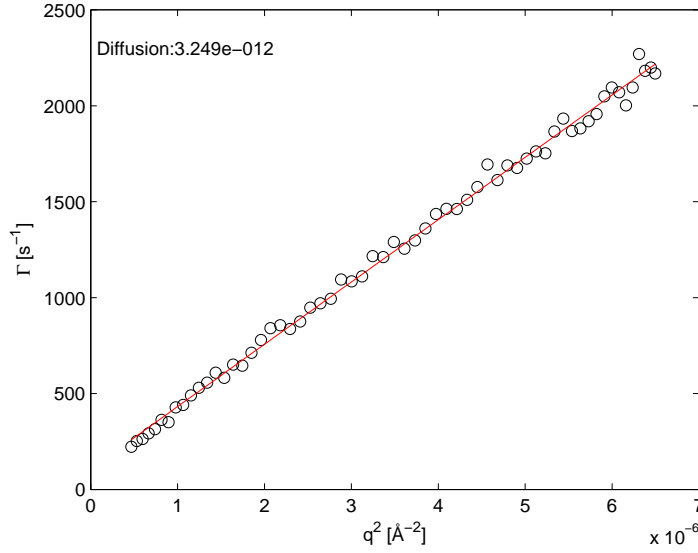


Figure 5.16:  $\Gamma(q^2)$  for the  $200\mu\text{M}$  FLSiMa070507 sample. From the slope of the function we can obtain the diffusion constant  $D_0$ .

Figure 5.17 shows  $S(q)$  and  $D_0/D(q)$  that we then obtained for the  $5\mu\text{M}$ -sample.

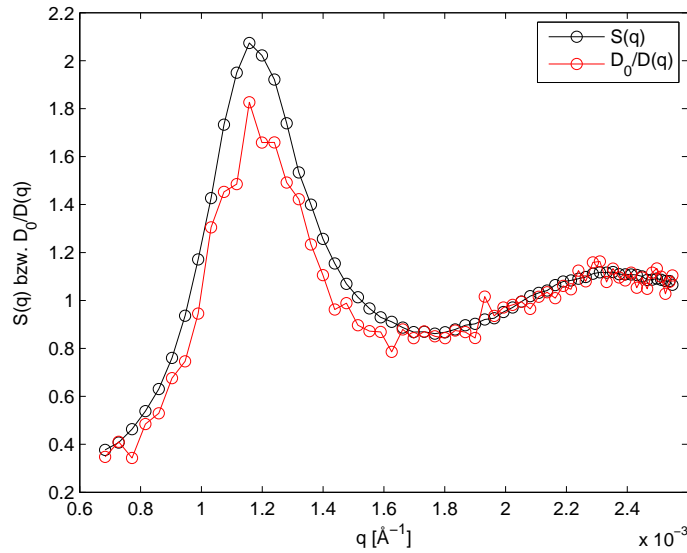


Figure 5.17:  $S(q)$  and  $D_0/D(q)$  of the  $5\mu\text{M}$ -sample.

Now we can obtain the hydrodynamic function  $H(q)$  simply by dividing these two functions by each other. The result is shown in figure 5.18.

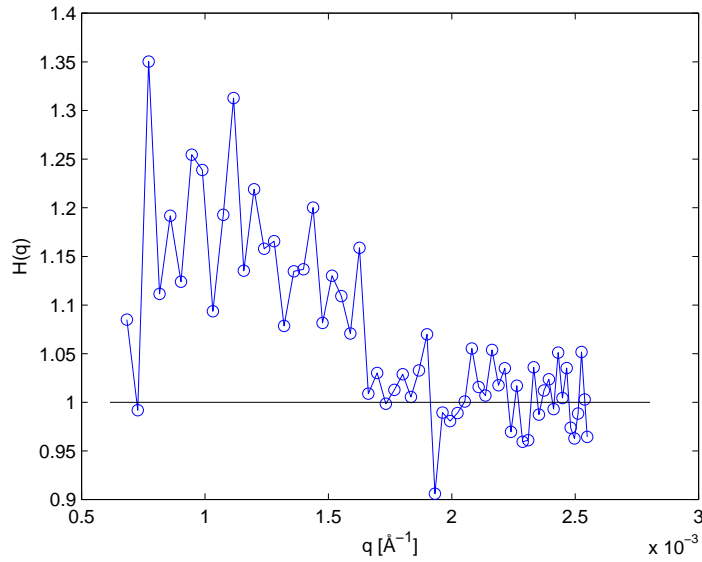


Figure 5.18: The hydrodynamic function  $H(q)$  for the  $5\mu\text{M}$ -sample.

As one can see from the plot, the interactions transmitted over the solvent disappear for high values of  $q$ .

The figures 5.19-5.22 show  $S(q)$  and  $D_0/D(q)$  that we obtained for the 20 – 100 $\mu\text{M}$ -samples.

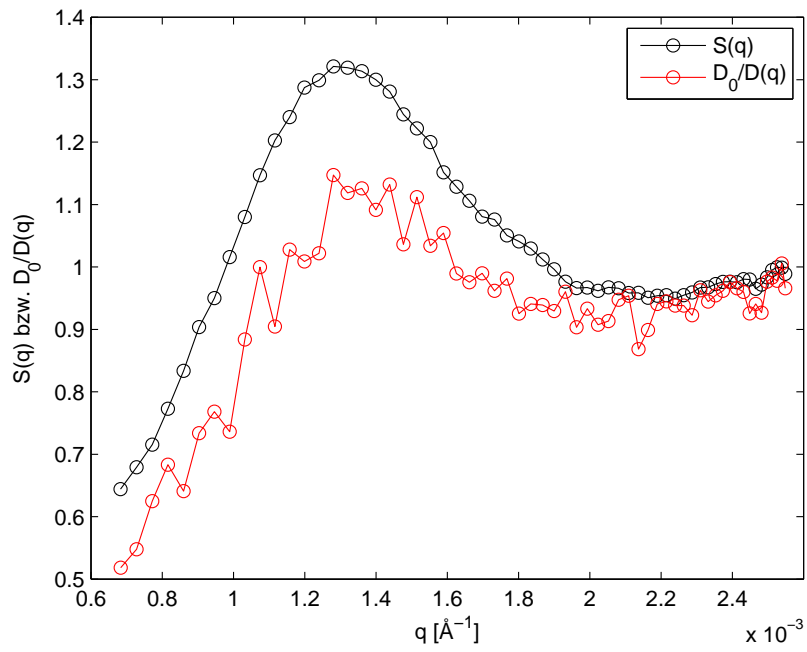


Figure 5.19:  $S(q)$  and  $D_0/D(q)$  of the  $20\mu\text{M}$ -sample.

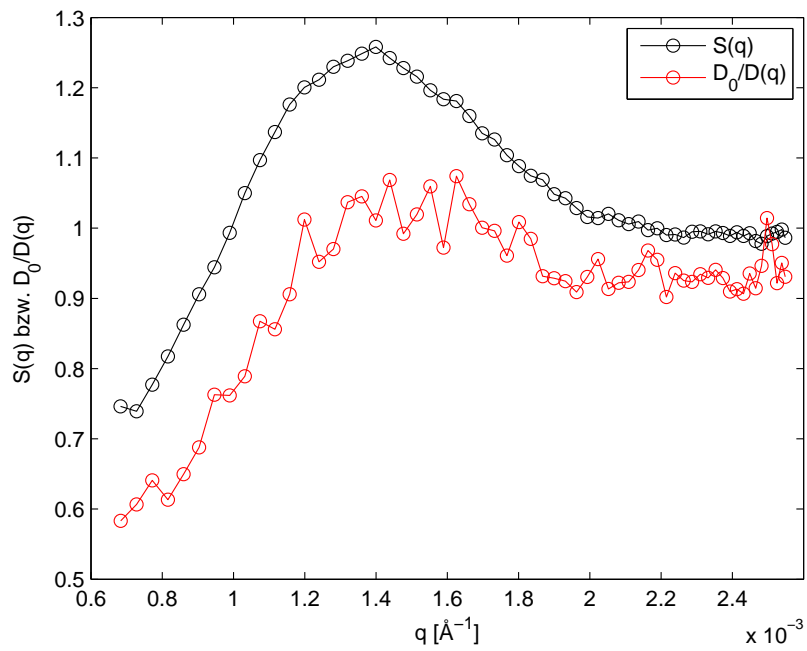


Figure 5.20:  $S(q)$  and  $D_0/D(q)$  of the  $50\mu\text{M}$ -sample.

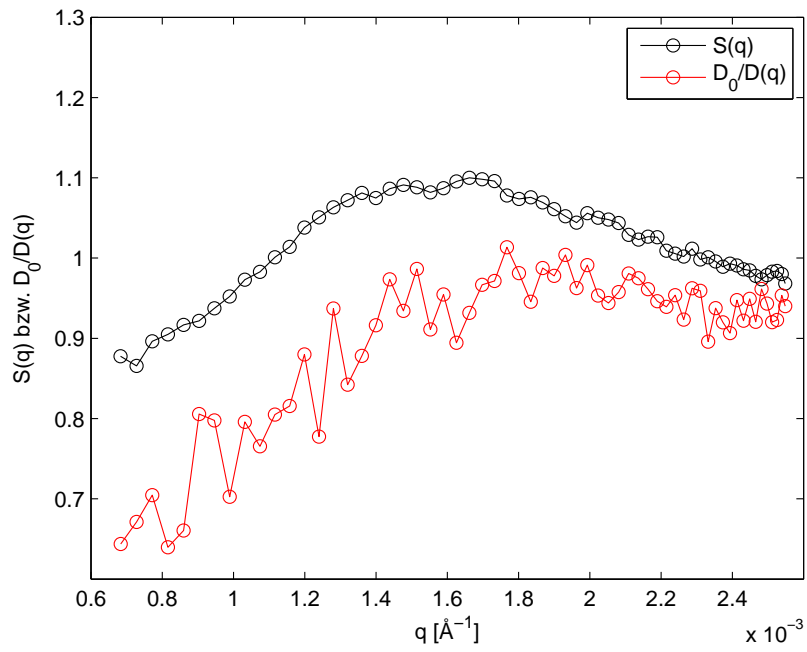


Figure 5.21:  $S(q)$  and  $D_0/D(q)$  of the  $75\mu\text{M}$ -sample.

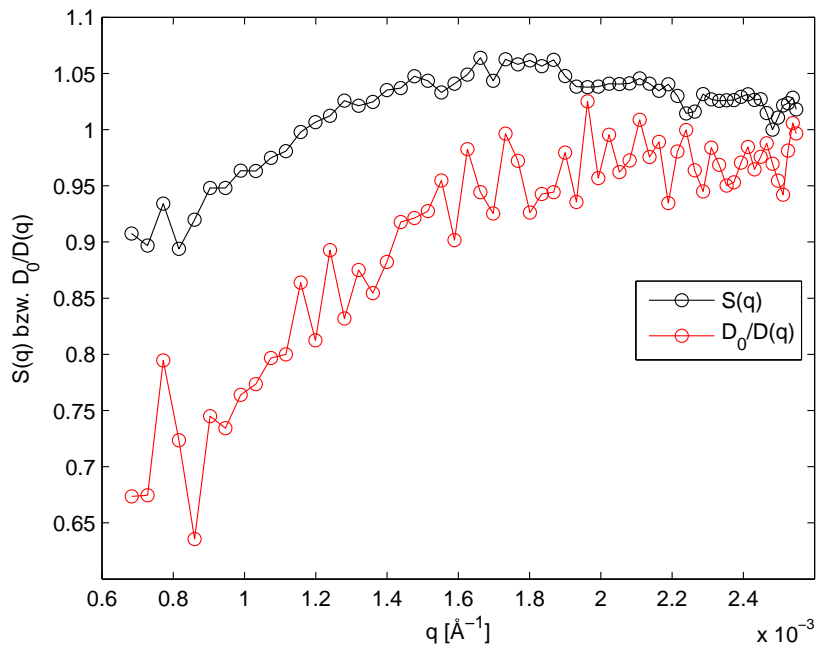


Figure 5.22:  $S(q)$  and  $D_0/D(q)$  of the  $100\mu\text{M}$ -sample.

Figure 5.23 shows an overview of the hydrodynamic functions we obtained for samples with different concentrations of KCl.

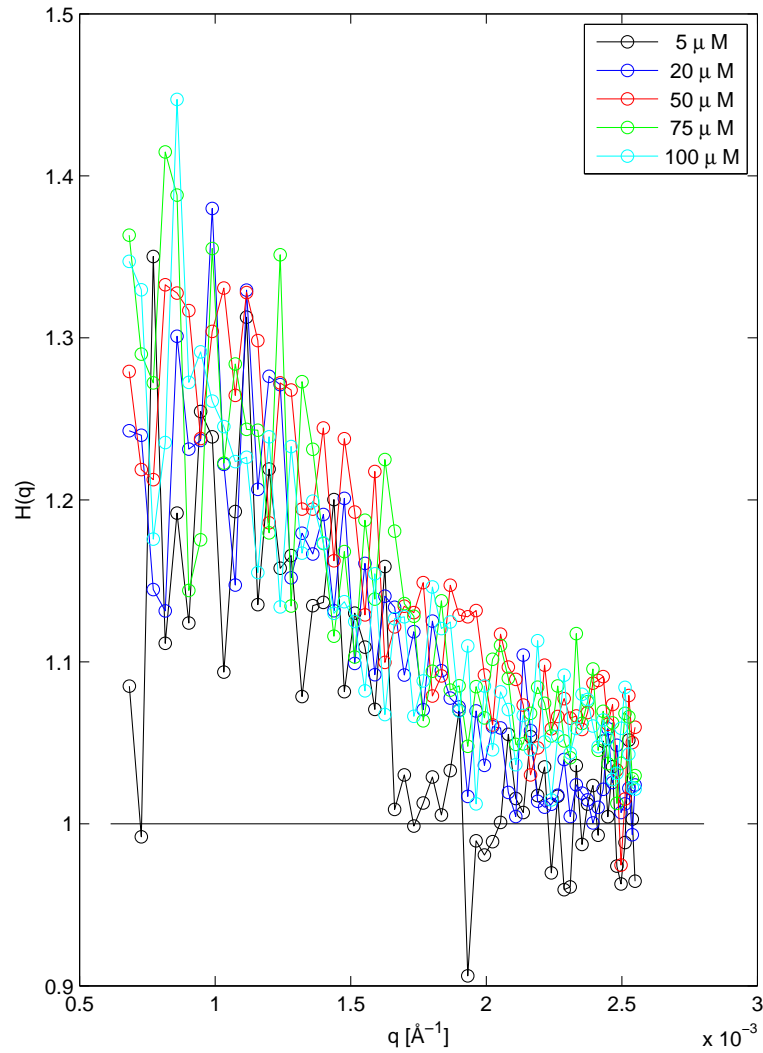


Figure 5.23: The hydrodynamic functions  $H(q)$  for the FlSiMa-samples with concentrations of KCl in the range of  $5\mu\text{M} - 200\mu\text{M}$ .

Considering the measuring accuracy one can say that there is no dependency of the hydrodynamic function  $H(q)$  on the salt concentration. A way to improve the results would be to extend the measuring time and to shorten the step between the measured angles. Fitting the  $\Gamma(q^2)$ -function before calculating  $D(q)$  from it is another possibility to improve the result for  $H(q)$ .

## 6 Conclusion

In our work, we used dynamic light scattering to gain insight into the structure and the dynamics of colloidal FLSiMa- and SiO<sub>2</sub>-systems.

We investigated the influence of ions in the solvent on the radius of the particles by preparing samples with different concentrations of KCl. For the FLSiMa-systems, we found out that the radius of the particles is decreasing with the increasing concentration of salt. Since we didn't have the possibility to measure the viscosity of our samples, we weren't able to figure out if our calculations were just a result of a change in the viscosity. For the SiO<sub>2</sub>-system, we couldn't find out any connection between the concentration of salt and the radius of the particles.

The investigation of the structure factor showed us that we were always dealing with liquid systems. From the value of  $q_{\max}$  we were able to figure out that the equilibrium distance between the colloidal particles decreases when one increases the concentration of salt in the sample. We ascribed this to the attenuation of the COULOMB potential that the particles feel when it gets screened by the ions. We were also able to figure out a lower correlation length for the samples with higher salt concentrations. Again, we considered the screened COULOMB potential to be responsible for this phenomenon since the long-distance effect of the particle interactions is very likely to disappear for high salt concentrations and the VAN-DER-WAALS interaction comes to the fore.

Concerning the hydrodynamic interactions in the samples, we found out that they disappear for high values of  $q$ . When regarding samples with different concentrations of salt, we couldn't find out any difference in the behaviour of the hydrodynamic function.

We acknowledge Agnes Duri, Christian Gutt and Fabian Westermeier for their support and collaboration during our work at Hasylab. We had a very nice and informative time and enjoyed the time in the workgroup.

## List of Figures

2.1	Stabilization processes: entropic repulsion and COULOMB repulsion	4
2.2	Constitution and structural formulae of Tetraethoxysilane (TEOS)	6
3.3	Standard scattering experiment . . . . .	7
3.4	Static structure factor . . . . .	10
3.5	Form factor of a homogenous sphere . . . . .	12
3.6	Fluctuating intensity and autocorrelation function . . . . .	14
3.7	Example of a measured $g_2 - 1$ function. . . . .	16
4.8	Experimental setup . . . . .	18
5.9	$\Gamma(q^2)$ for <i>FlSiMa020507</i> (200 $\mu$ M KCl) . . . . .	19
5.10	R(C) for <i>FlSiMa020507</i> . . . . .	20
5.11	R(C) for <i>FlSiMa110708</i> . . . . .	21
5.12	R(C) for <i>SiO<sub>2</sub>280708</i> . . . . .	22
5.13	$\langle I(q) \rangle$ of <i>FlSiMa070507</i> (5 $\mu$ M and 200 $\mu$ M KCl) . . . . .	24
5.14	$S(q)$ for <i>FlSiMa070507</i> (5 $\mu$ M – 200 $\mu$ M KCl) . . . . .	25
5.15	$\Gamma(q^2)$ for <i>FlSiMa070507</i> (5 $\mu$ M KCl) . . . . .	27
5.16	$\Gamma(q^2)$ for <i>FlSiMa070507</i> (200 $\mu$ M KCl) . . . . .	28
5.17	$S(q)$ and $D_0/D(q)$ for <i>FlSiMa070507</i> (5 $\mu$ M KCl) . . . . .	28
5.18	$H(q)$ for <i>FlSiMa070507</i> (5 $\mu$ M KCl) . . . . .	29
5.19	$S(q)$ and $D_0/D(q)$ for <i>FlSiMa070507</i> (20 $\mu$ M KCl) . . . . .	30
5.20	$S(q)$ and $D_0/D(q)$ for <i>FlSiMa070507</i> (50 $\mu$ M KCl) . . . . .	30
5.21	$S(q)$ and $D_0/D(q)$ for <i>FlSiMa070507</i> (75 $\mu$ M KCl) . . . . .	31
5.22	$S(q)$ and $D_0/D(q)$ for <i>FlSiMa070507</i> (100 $\mu$ M KCl) . . . . .	31
5.23	$H(q)$ for <i>FlSiMa070507</i> (5 $\mu$ M – 200 $\mu$ M KCl) . . . . .	32